Nested multi-resolution PIV measurements of wall bounded turbulence at high Reynolds numbers

C. M. de Silva[1], **C. Atkinson**[2], **N. A. Buchmann**[2], **E.P. Gnanamanickam**[1], **N. Hutchins**[1], **J. Soria**[2,3] **and I. Marusic**[1]

[1]Department of Mechanical Engineering, The University of Melbourne, Victoria 3010, Australia.

[2]Laboratory for Turbulence Research in Aerospace & Combustion, Department of Mechanical and Aerospace Engineering, Monash University, Victoria 3800, Australia.

[3]Department of Aeronautical Engineering, King Abdulaziz University, Jeddah, Kingdom of Saudi Arabia.

ABSTRACT

Here we describe the use of a nested high magnification camera configuration within a large field of view (FOV) PIV experiment. The objective of these measurements is to obtain instantaneous velocity flow fields to resolve the wide range of scales present in turbulent boundary layers at high Reynolds numbers of up to $Re_\tau \approx 20000$. Flow statistics are compared against previous measurements made using hot-wire anemometry to validate and assess the quality of the PIV velocity fields. Preliminary analysis shows that the instantaneous wall shear stress can be computed from the experimental data, enabling us to directly compute quantities such as the friction velocity.

1. Introduction

Particle image velocimetry (PIV) has become increasingly popular over the last decade for accurately measuring multi-component, multi-dimensional velocity fields associated with turbulent flows. More recently, due to the advancement and increase in resolution of PIV cameras, studies have shown that PIV techniques can be effectively applied with spatial resolutions of the order of a few microns [Kahler et al., 2012]. Here we describe the application of such a technique to simultaneously obtain a large FOV while also resolving the small scales in the near wall region of a high Reynolds number turbulent boundary layer by using varying magnifications. The application to high Reynolds number flows further emphasises the importance of having varying resolutions; a large FOV is necessary to capture the larger structures, which scale with the boundary layer thickness ($\approx 0.35m$). Conversely, the smaller scales associated with the near wall cycle scale with inner viscous units ($\nu/U_\tau \approx 45\mu$m at $Re_\tau \approx 8000$) and require high spatial resolution.

The novelty of the data-set presented is the ability to obtain well resolved instantaneous velocity fields at close proximity to the wall (approaching the viscous sublayer), within a large FOV. This enables us to quantitatively analyse large scale structures in the logarithmic and outer regions of the boundary layer and their associated modulating effect on near wall structures [Marusic et al., 2010].

Here, we use the coordinate system x, y and z to refer to the streamwise, spanwise and wall-normal directions respectively. The instantaneous stream-wise velocity and wall-normal velocity are represented by $\widetilde{U}$ and $\widetilde{W}$ respectively, with corresponding fluctuating velocity components given by u, v and w. Capitalisation and overbars indicate averaged quantities. The superscript + refers to normalisation with the inner scales. For example, we use $l^+ = lU_\tau/\nu$ for length and $U^+ = U/U_\tau$ for velocity, where U_τ is the friction velocity and ν is the kinematic viscosity of the fluid.

2. Experimental setup

The experiments are performed in the High Reynolds Number Boundary Layer Wind Tunnel (HRNBLWT) at the University of Melbourne. Figure 1 shows an overall view of the experimental setup which is located 21m downstream of the trip. The long development length enables us to obtain high Reynolds numbers at relatively slow freestream velocities, which results in a larger viscous length scale, and hence less acute spatial resolution issues. The imaging system used to obtain the large field of view (FOV) of approximately 0.8m × 0.5m (detailed further in de Silva et al. [2012]) consists of eight PCO4000 cameras (4008 × 2672 pixels, 2Hz) arranged as shown in figure 1. It is desirable to capture the large scale structures that have length scales the order of the boundary layer thickness (δ) with a large FOV. Meanwhile the use of multiple cameras enables us to maintain adequate spatial resolution to resolve most of the smaller length scales, which are the order of the Kolmogorov length scales (η). At high Reynolds numbers this task is further complicated since the ratio δ/η is large ($\approx 10^3$ for the flow studied here). To overcome this, a higher magnification is used in the near-wall and log region where we expect a larger contribution of the turbulent energy to be from small scales. Meanwhile for the outer region, a lower magnification is used that is capable of resolving the dominant larger scale structures prevalent here. The novelty of the measurements presented here is the use of a ninth PCO4000 camera simultaneously to obtain a highly magnified (High-mag) view in the near wall region, which is nested within the larger FOV (shown in figure 2).

The particles are illuminated by two laser sheets overlapped in the spanwise direction, and created using two Spectra Physics 'Quanta-Ray' PIV 400 Nd:YAG double-pulse lasers that deliver 400mJ/pulse. One laser is dedicated to illuminating the large FOV, and the second
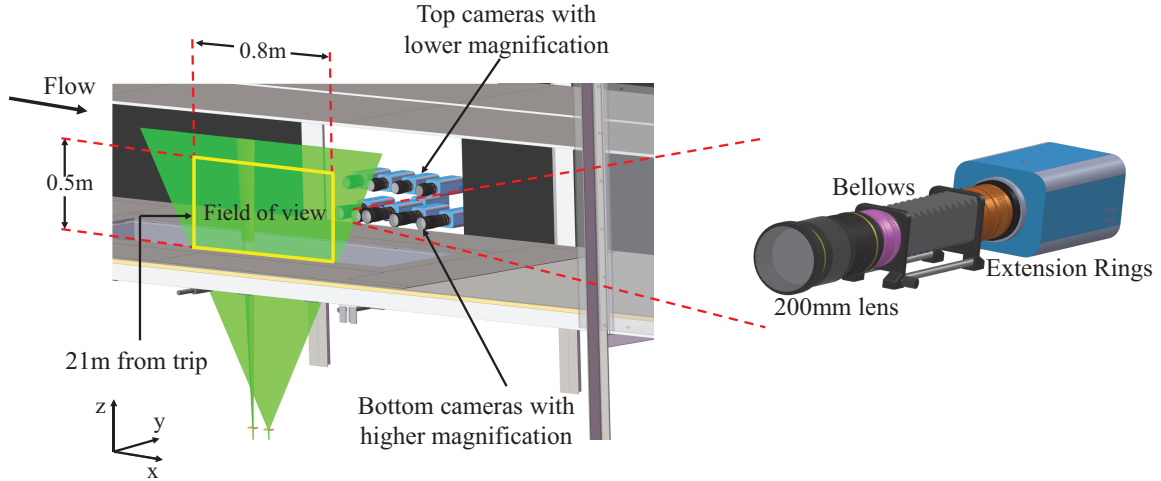
Figure 1: Experimental setup used to conduct planar PIV experiments in the HRNBLWT. (left) The camera setup in the facility to obtain the large field of view (FOV),simultaneously with the High-mag view using a second laser sheet and high magnification optics on a ninth camera. (right) A scaled schematic of high magnification camera H_1.

laser is used for the highly magnified small FOV in the near wall region. The necessity for a large amount of concentrated power for the high magnification camera (H_1) is primarily due to the loss of light through the optical configuration used (shown in figure 1(right)), where the object distance is ≈ 1m and the FOV spans $\approx 0.03\text{m} \times 0.02$m. We employ a bellows, tele-converter and a series of extension tubes to obtain the necessary magnification rather than simply employing a long-range microscope such as Infinity-K2 [Kahler et al., 2012]. This approach is adopted due to the large sensor size of the PCO4000 camera. The use of multiple lasers to illuminate vastly different magnifications posses a few issues. Firstly, due to the significantly higher intensity of the smaller laser sheet, it is slightly offset in time to avoid saturating the large FOV cameras. The time offset between the laser sheets is such that within this range the flow field can be considered to be frozen (in the order of $t^+ \approx 0.5$ at $Re_\tau \approx 8000$). However, the time offset is known, therefore it can be accounted for when stitching the images together.

The experimental data is processed using an in-house PIV package, similar that used in de Silva et al. [2012]. For the data presented in this paper an interrogation window size of 32×32 pixels was used for the bottom and top cameras at $Re_\tau \approx 8000$, which corresponds to an interrogation window size of approximately 34 wall units for the bottom cameras and 45 wall units for the top cameras. For the higher speeds to improve the spatial resolution or at minimum retain an equivalent resolution obtained for the lower Reynolds number data, we attempt to use smaller interrogation window sizes as summarised in table 1. The high magnification view H_1 has a pixel size of approximately 7.5µm, which corresponds to a interrogation window size of approximately 4×4 wall units at 32×32 pixels, thus enabling us to adequately resolve the small-scales present in the flow. Measurements are conducted at three freestream velocities, which include 10, 20 and 30m/s, with corresponding Reynolds numbers based on friction velocity of $Re_\tau = u_\tau \delta / \nu \approx 8000$, 14500 and 19500. To maintain the same vector spacing we determine the vector grid in real space with an overlap of 50% for the bottom cameras, while the vector spacing for the top camera is matched with the spacing of the bottom cameras. The vector spacing for the three speeds considered is summarised in table 1. The vectors are mapped to real space using a calibration process to perform the cross-correlation. Meanwhile, for the High-mag view the vector spacing is two wall units at 50% overlap, in the order of most direct numerical studies.

Table 1: Summary of parameters of the experimental data. The interrogation window sizes are given in viscous units, and the highlighted numbers in red corresponds to the data presented in this study.

U_∞ (ms^{-1})	Re_τ	ν/U_τ (µm)	Interrogation window size				
			Bottom Camera l^+		Top Camera l^+		High-mag l^+
			16×16	32×32	24×24	32×32	32×32
10	8000	45	17	34	33	45	5
20	14500	24	32	64	62	83	10
30	19500	17	44	88	87	117	14

3. Calibration procedure

Planar PIV measurements are typically calibrated by using a pixel to real space conversion based on a scaling factor determined using an *in situ* calibration, which may simply be performed by the imaging of a scale. However, even planar PIV images are typically affected to a certain degree by perspective and optical distortion from the optics, particulary when the FOV is large and misalignments often exist between the image plane and laser sheet [Adrian and Westerweel, 2011]. This error is typically considered to be minimal in planar PIV, but can be significant when the field of view is large. To correct distortions present in the images, a similar approach to that performed by de Silva et al. [2012] is adopted for the large FOV, where a large calibration grid which spans the length of the complete FOV is used. This grid is then used to determine calibration coefficients which map each camera's pixel space (X, Y) to real space (x, y). In addition, this calibration accounts for misalignments in camera positioning and enables us to stich the velocity field from
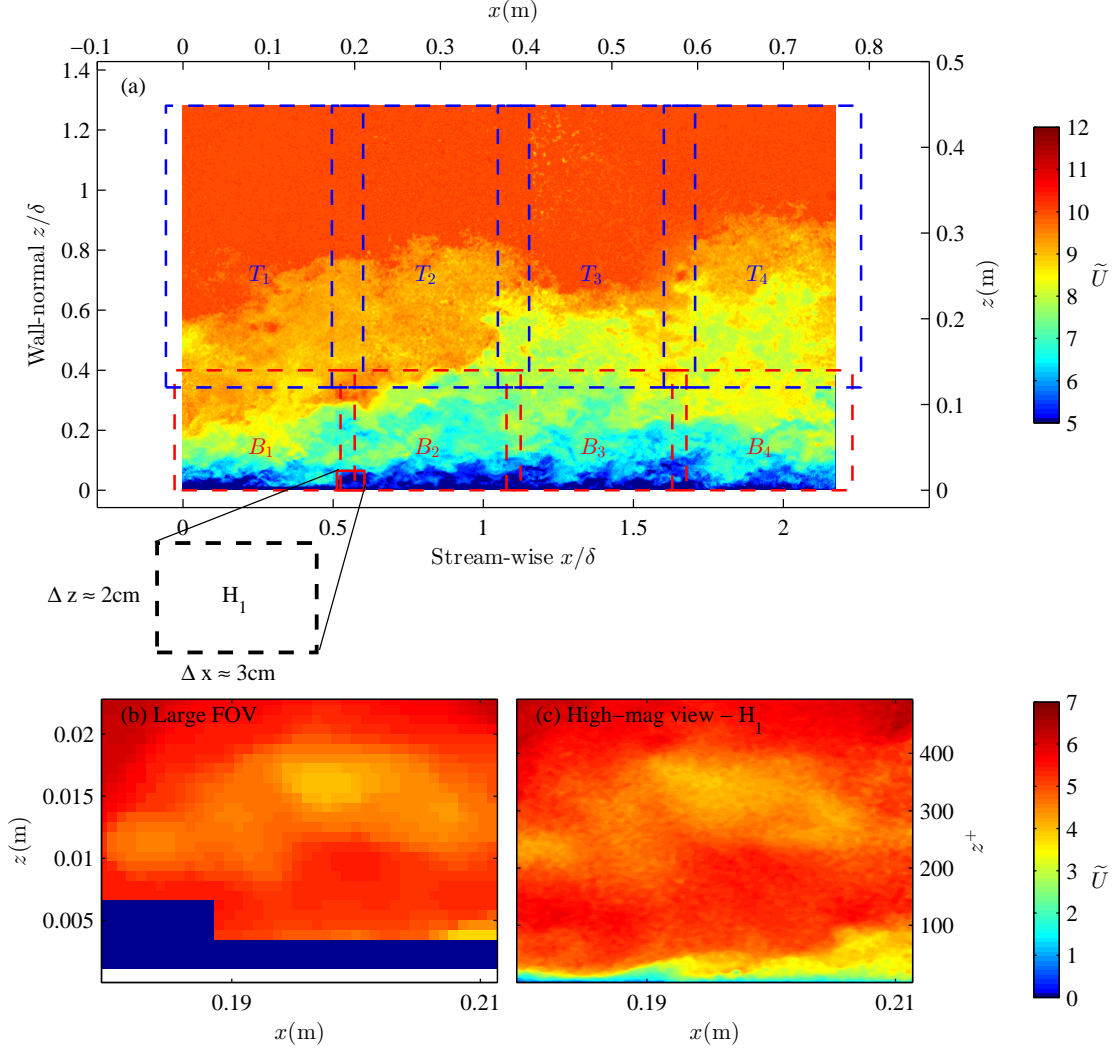
Figure 2: (a) shows the FOV across the eight cameras (L_{1-4} and T_{1-4}), H_1 indicates the location of the high magnification view nested within the larger FOV in the near wall region. The location $x = 0$ is located 21m downstream of the trip. (b) Shows the instantaneous streamwise velocity vectors seen by the large FOV in the region captured by H_1, meanwhile (c) shows the same region as seen with the high magnification camera.

multiple cameras by precisely locating each camera's position relative to the others. The calibration grid used for the large FOV has a grid spacing of 5mm. However for the High-mag view, which only spans a few centimeters in width a smaller machined calibration grid with 1mm spacing was necessary.

Precisely locating the wall position is a key issue for most measurements in wall-bounded flows, and is particularly so when considering a streamwise wall-normal plane in PIV experiments due to wall reflections caused by the laser sheet [Adrian and Westerweel, 2011]. Here we use the calibration grid to assist us in locating the wall location relative to the four lower cameras, using the reflection of the calibration grid on the glass wall and the estimated pixel position of the wall in each camera (detailed further in de Silva et al. [2012]). It should be noted that similar to the calibration process detailed previously it is essential to first map the image to real space using the calibration coefficients prior to computing the estimated wall position. This method was previously shown to work well for a similar large FOV experiment [de Silva et al., 2012]. Here we extend this technique and conclude that a similar technique provides acceptable accuracy for the highly magnified view, based on the mean streamwise velocity (shown in figure 3(a)), which is obtained without applying any shift to the wall position of the velocity fields. However, we note that there can be very small errors in relation to the positioning of the calibration target and imperfections on the glass wall, but results indicate this error to be well below 100μm (as evidenced by the collapse of the mean velocity profile to $z^+ < 3$).
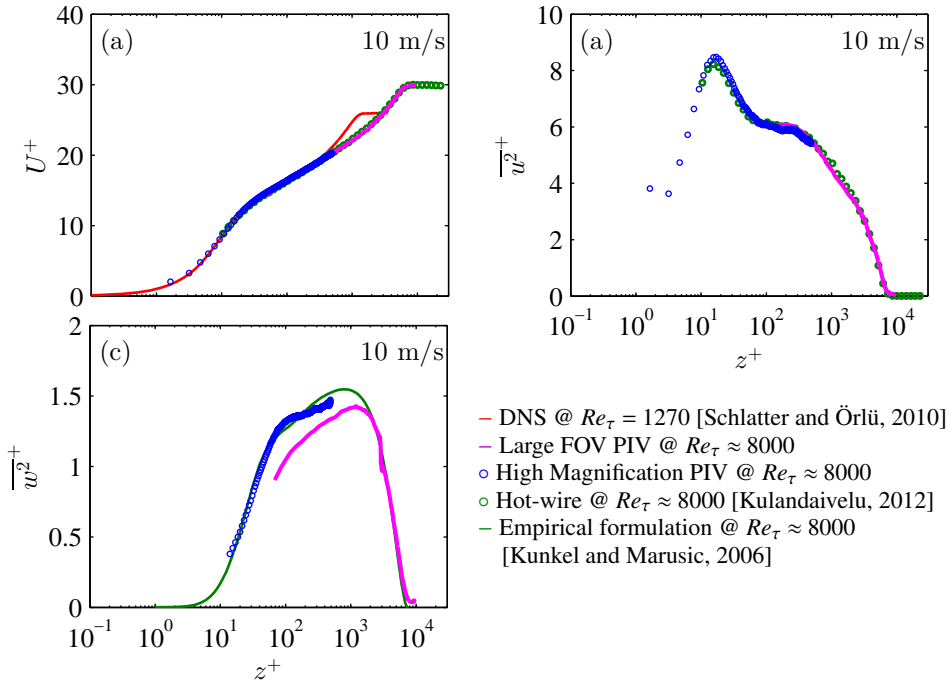
4. Results

4.1 Mean and turbulence intensity flow statistics

The main novelty in the measurements detailed is the range of magnifications simultaneously employed to resolve the range of scales present in a high Reynolds number flow. Figure 2a shows the layout of all the nine cameras, with contours of instantaneous streamwise

velocity overlayed. Figure 2(a) gives a good visual indication of the range of length scales associated with such high Reynolds number flows. Figure 2(b) shows a cut out of the large FOV which is simultaneously captured by the high magnification camera (shown in figure 2c). Comparisons between figure 2(b) and 2(c) clearly shows the loss of small scale information in the large FOV, in addition to the lack of reliable data below a wall position of 75 wall units in z which is also evident in the flow statistics shown in the later part of this paper. We see that the High-mag view is resolved much better and also has reliable velocity vectors significantly closer to wall.

Extensive comparisons of mean flow (U^+) and turbulence intensity ($\overline{u^2}^+$ and $\overline{w^2}^+$) flow statistics between the PIV measurements and hot-wire anemometry measurements from the same facility at matched Reynolds numbers is summarised in de Silva et al. [2012] at a Reynolds number of $Re_\tau \approx 8000$. A good agreement has been observed between the planar PIV measurements and the hot-wire anemometry using the large FOV. However, it was evident that the near wall region ($z^+ < 90$ at $Re_\tau \approx 8000$) is not captured well in the PIV measurements due to issues such as the reflection from the wall. This is also evident in our current set of measurements ($z^+ < 75$ at $Re_\tau \approx 8000$), if we only consider the large FOV as observed in figure 2(b).

Figures 3(a) and 3(b) shows streamwise mean velocity and turbulence intensity profiles from the current PIV measurements (Large FOV in – and the High-mag view ◦) compared with hotwire measurements (◦ symbols) at an equivalent Reynolds number. Preliminary results indicate that the High-mag view provides instantaneous velocity measurements to within a few wall units ($1 - 3$) from the wall, which is encouraging. For example, we can clearly see the inner peak at ($z^+ = 15$) in $\overline{u^2}^+$ using the High-mag view. Owing to the spatial resolution attained we see minimal impact from spatial averaging at $Re_\tau \approx 8000$, as one would expect, since the interrogation window size in x and z is approximately four viscous units. However, we note that planar PIV measurements are also spatially averaged in the y direction as a result of the laser sheet thickness. In this case, due to the small depth of focus (less than five wall units at $Re_\tau \approx 8000$) for the High-mag view, this effect is also minimised. However, for the larger FOV the effect of spatial averaging is more adverse, due to the significantly larger interrogation window size, which is evident at the higher Reynolds numbers considered in this study. In fact, we expect larger attenuation for the PIV measurements due to the three dimensional averaging in comparison to hotwire measurements, which are spatially averaging in the spanwise direction over the wire length $l^+ \approx 22$ [Hutchins et al., 2009]. This is not evident in the current results at the lower Reynolds numbers considered, since we cannot resolve the near wall region in the large FOV planar PIV measurement ($z^+ < 75$). Furthermore, we believe that the near wall-region obtained from PIV data may be affected by noise, particularly for the large FOV due to poor image quality very close to the wall; this would cause the turbulence intensity to increase and reduce the discrepancy present.

Figure 3: Comparison of planar PIV results with results from hot-wire anemometry experiments and empirical formulations at $Re_\tau \approx 8000$ for flow statistics U^+, $\overline{u^2}^+$ and $\overline{w^2}^+$. The green ◦ symbols represent the hotwire data, the solid magenta line (–) indicates the Large FOV PIV and the blue ◦ symbols correspond to the High-mag PIV. The solid red line (–) for U^+ is obtain from direct numerical simulation data at $Re_\tau = 1270$ [Schlatter and Örlü, 2010], and the solid green (–) line in (c) is a predicted profile from an empirical formulation at an equivalent Reynolds number.
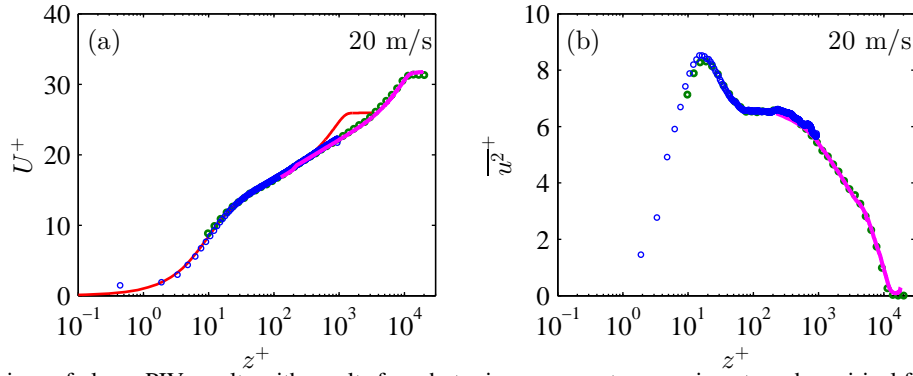
Figure 4: Comparison of planar PIV results with results from hot-wire anemometry experiments and empirical formulations at $Re_\tau \approx 14500$ for flow statistics U^+ and $\overline{u^2}^+$. Symbols are defined in figure 3.

Next we consider $\overline{w^2}^+$, shown in figure 3(c). Since there are limited experimental data at the Reynolds numbers considered in this study, comparisons are drawn against empirical formulations based on experimental data spanning three decades of Reynolds numbers [Kunkel and Marusic, 2006, Perry et al., 2002]. Results indicate greater discrepancy for $\overline{w^2}^+$ compared to $\overline{u^2}^+$, which can be attributed to the smaller scales associated with $\overline{w^2}^+$ causing larger spatial attenuation in the large FOV. This can be confirmed by the fact that the High-mag view shows much better collapse.

4.2 Viscous sublayer - Near wall region

The high magnification camera enables us to obtain reliable instantaneous velocity vectors in close proximity to the wall within the viscous sublayer ($z^+ < 5$) even at the high Reynolds numbers $O(10^4)$ considered in this paper. We note that prior hotwire measurements in the same facility have not yet been able to capture this region, making the results presented here novel for a zero pressure gradient turbulent boundary at these Reynolds numbers. (with the exception of results presented by Kahler et al. [2012] at similar Reynolds numbers). Figure 5 shows the instantaneous streamwise velocity obtained from the high magnification camera with the ordinate shown in logarithmic space. Qualitatively it is evident that the measurement is providing a velocity field within the viscous sublayer. This enables us to compute quantities such as the instantaneous wall shear stress τ_w and the friction velocity U_τ directly from the instantaneous velocity gradient $\partial U/\partial z$. At $Re_\tau \approx 8000$ we obtain $U_\tau \approx 0.332$, which is within 0.5%, of the Monkewitz et al. [2007] prediction based on oil film interferometry measurements. The friction velocities obtained at the three speeds considered can be compared to prior measurements of the same quantity in the same facility at the same streamwise location. For this we employ direct skin friction measurements obtained from a drag balance [Talluru et al., 2010] and prior measurements by Hutchins et al. [2009] where U_τ is obtained using a using a Clauser chart method with logarithmic law constants of $\kappa = 0.41$ and $A = 5$. Figure 6(a) shows good collapse between the three independent measurements considered for U_τ, with the PIV measurements from this study extending results up to 30ms^{-1}. Figure 6(b) shows the skin-friction coefficient c_f from the PIV measurements compared against empirical relations for c_f developed in Nagib and Monkewitz [2007], in addition to measurements from the drag balance facility at the HRNBLWT. Figure 6(b) shows that our prediction from the PIV measurements has good collapse on the empirical formulations. In fact, we see a significantly lower variation in comparison to measurements from the drag balance facility.
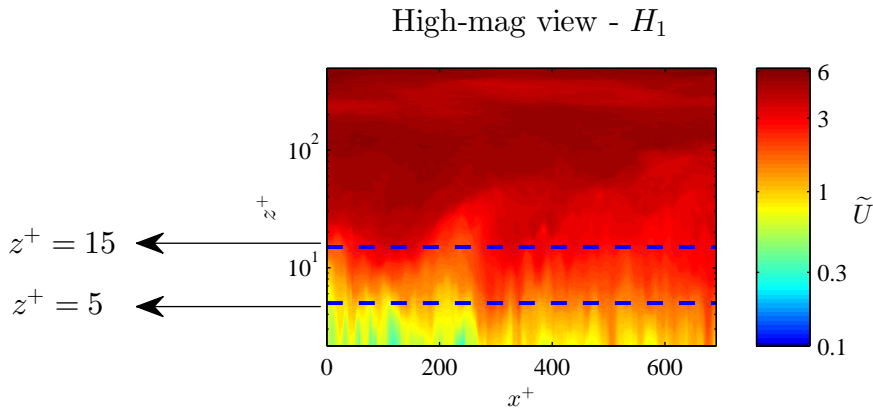
Figure 5: Colour contours of instantaneous streamwise velocity obtained from the high magnification camera with the ordinate shown in logarithmic space to emphasise the near wall region. The dashed lines indicate the start of the viscous sublayer ($z^+ < 5$) and the location of the inner peak in the streamwise turbulence intensity.
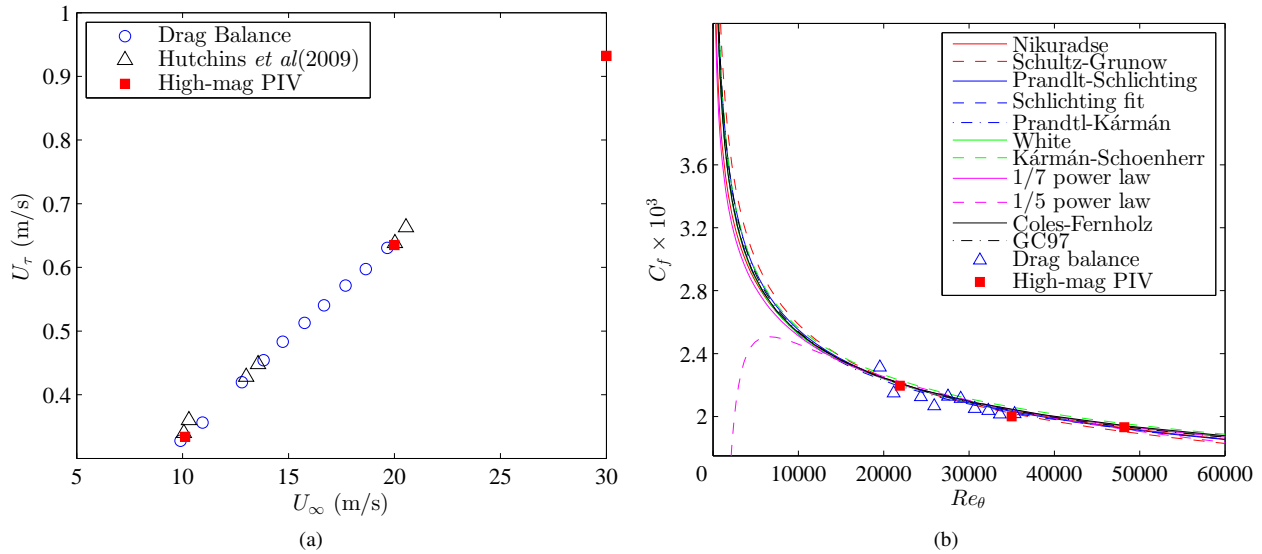
Figure 6: (a) Comparison of U_τ with U_∞ from the High-mag PIV experiment compared with prior results from a drag-balance [Talluru et al., 2010] and Clauser chart results of Hutchins et al. [2009] in the same facility at the same streamwise position. (b) Comparison of c_f values with established empirical relations for c_f with Re_θ [Nagib and Monkewitz, 2007].

5. Conclusion

An assessment is presented on the application of a large FOV multi-camera planar PIV measurement simultaneously with a high magnified view. For the large FOV we also use multiple magnifications, where a higher magnification is used for the near wall and log region to assist in resolving the small scales, and a relatively lower magnification is used in the outer region. Results indicate that the combination of multiple magnifications works well, enabling us to resolve a wide range of scales present in flows at high Reynolds numbers in comparison to using a single magnification. This is verified by comparing first and second order flow statistics from the PIV velocity fields with hot-wire anemometry measurements from the same facility. This comparison indicates that the PIV measurements are promising. The inclusion of the highly magnified view enables us to resolve the near wall region up to a few wall units $(1 - 3)$ from the wall. This enables us to directly determine quantities such as the friction velocity, which is typically found using empirical fits. Results indicate that the viscous sublayer region is resolved to within acceptable accuracy. We note that the measurement can be extended to perform conditional statistics between the small scale features observed in the near-wall region and the overlying larger structures in the outer regions, which would be in the order of δ. Furthermore, we note that in the measurements presented here we can compute the instantaneous wall shear stress fluctuations (a quantity that has been traditionally challenging at high Reynolds numbers).

REFERENCES

R. J. Adrian and J. Westerweel. *Particle Image Velcimetry*. Cambridge University Press, 2011.

C. M. de Silva, K. A. Chauhan, C. H. Atkinson, N. A. Buchmann, N. Hutchins, J. Soria, and I. Marusic. Implementation of large scale piv measurements for wall bounded turbulence at high reynolds numbers. 18th Australasian Fluid Mechanics Conference, Launcheston, Australia, 3-7 December 2012, 2012.

N. Hutchins, T. B. Nickels, I. Marusic, and M. S. Chong. Hot-wire spatial resolution issues in wall-bounded turbulence. *J Fluid Mech*, 635:103–136, 2009.

C. J. Kahler, S. Scharnowski, and C. Cierpka. High resolution velocity profile measurements in turbulent boundary layers. 16th Int Symp on Applications of Laser Techniques to Fluid Mechanics, Lisbon, Portugal, 09-12 July, 2012.

V. Kulandaivelu. *Evolution of zero pressure gradient turbulent boundary layers from different initial conditions*. PhD thesis, The University of Melbourne, 2012.

G.J. Kunkel and I. Marusic. Study of the near-wall-turbulent region of the high-Reynolds number boundary layer using an atmospheric flow. *J. Fluid Mech.*, 548:375–402, 2006.

I. Marusic, B. J. McKeon, P. A. Monkewitz, H. M. Nagib, A. J. Smits, and K. R. Sreenivasan. Wall-bounded turbulent flows at high reynolds numbers: Recent advances and key issues. *Physics of Fluids*, 22(6):065103, 2010.

P. A. Monkewitz, K. A. Chauhan, and H. M. Nagib. Self-consistent high-reynolds-number asymptotics for zero-pressure-gradient turbulent boundary layers. *Physics of Fluids*, 19(11):115101, 2007.

Chauhan K. A. Nagib, H. M. and P. A. Monkewitz. Approach to an asymptotic state for zero pressure gradient turbulent boundary layers. *Phil. Trans. R. Soc. A*, 365:755–770, 2007.

A. E. Perry, I. Marusic, and M. B. Jones. On the streamwise evolution of turbulent boundary layers in arbitrary pressure gradients. *J. Fluid Mech.*, 461:61–91, 2002.

Philipp Schlatter and Ramis Örlü. Assessment of direct numerical simulation data of turbulent boundary layers. *Journal of Fluid Mechanics*, 659(1):116–126, 2010.

K. M. Talluru, C. M. desilva, and I. Marusic. New drag balance facility for skin-friction studies in turbulent boundary layer at high reynolds numbers. *Proc. 17th Australasian Fluid Mech. Conference*, 2010.